University of Thi-Qar Journal Vol.14 No.2 June 2019
Web Site: https://jutq.utq.edu.iq/index.php/main
Email: journal@jutq.utq.edu.iq

Investigation of electronic properties of alloyed double metal ring

Samar M. Merdas, Lafy F. Al-Badry and Falah H. Hanoon
Email: albadrylafy@yahoo.com
Email: drfh24@yahoo.com
Department of Physics, Faculty of Science,
University of Thi Qar, Nassiriya 64000, Iraq

Abstract

The present work is a theoretical study of the electronic properties of alloyed double metal ring (ADMR) threaded by magnetic flux. The system that takes into account in the study is consisting of two rings connected parallel, with two different types of atomic sites. This work having; two parts. The first part a calculation of the energy spectrum, persistent current, Drude weight and low-field magnetic susceptibility of ADMR by the tight-binding method. While the second part is a is a computation of electronic properties of the alloyed double metal ring by density functional theory (DFT). The latter part is considered as a simulation of what was studied in the first part. The results, of our proposed work show that the on-site energies for both types of atoms, inter-ring coupling strength and hopping strengths play an important role in controlling the electronic properties.

Keywords*:* persistent current; double metal ring; Drude weight; DFT.

1. Introduction

Over the last few decades, the phenomenon of a persistent current in mesoscopic ring systems has received much attention because it's an important role in understanding quantum coherence in such ring systems. Quantum interference phenomena hase been observed in mesoscopic ring systems in the presence of a magnetic flux, such as the Aharonov-Bohm effect in the persistent currents, which never decay with time. The persistent currents are generated from the quantum orbital motion of electrons in mesoscopic normal-metal rings threaded by a magnetic flux [1, 2].

Mesoscopic ring systems must have two important characteristics to obtain the persistent current. Firstly, the size of the system must be comparable to the phase coherence length of electrons. The secondly, the system must be at sufficiently low temperature. These two conditions arise from the fact that the average energy level spacing must be greater than the thermal energy. The average energy level spacing increases as the size of the system decreases and therefore the persistent current will flow in the mesoscopic ring systems. As a result, the discrete of energy levels plays important role in the flow persistent currents in mesoscopic rings [3, 4].

The basic idea of the persistent current in a normal metal ring was first proposed by Büttiker et al. in 1983 [5] and Büttiker in 1985 [6]. Several theoretical and experimental studies have achieved to investigate interesting characteristic features of persistent currents in different mesoscopic geometries. Most of the geometrical structures that studied are simple mesoscopic ring [3, 7-10], an array of mesoscopic rings [11], mesoscopic cylinder [12-14], Möbius strip [15]. In these studies, persistent currents have been calculated with respect to temperature [16, 17], electron–phonon interaction [18], electron correlation [19], Rashba and Dresselhaus spin-orbit interactions [20, 21] electric field [22].

In the last decade, it has also been possible to fabricate noble metals in different nanostructures such as metal rings [23, 24], nanowires [25], nanoplates [26] and nanotubes [27]. The high cost and difficulty of saving of noble metals made their use limited in nanotechnology. Mixing of noble metals with earth-abundant metals has improved their properties [28]. Alloyed noble metals have received special attention as a result of their extensive applications in the field of nanotechnology [29, 30]. Noteworthy that the alloyed Cu-Au [31], Au-Ag [32] and Cu–Ag [33] metals with much better properties than pristine metals have been synthesized for applications in several fields like electronics, optoelectronics and bio-sensing.

This work consists of two parts; the first part present an analytical method for studying the electronic properties of alloyed double metal ring subjected to an Aharonov-Bohm flux. All the electronic properties in this part, as the energy spectrum, persistent current, Drude weight and

magnetic susceptibility, are calculated by the tight-binding Hamiltonian without interacting electrons. While second part of this work, we present a computational study as simulate of the studied systems in the first part by using density functional theory (DFT). The equilibrium geometries, density of states and electronic properties of Cu_6Au_6, Cu_6Ag_6, and Ag_6Au_6 systems are computed.

The outline of this article is as follows: The theoretical model is presented in Sec. 2, including the model Hamiltonian of the ADMR. In Sec. 3, explaineded the computational details of the second part has been of this work. The results of the analytical and computational part are discussed in Sec. 4. The conclusion is dedicated to Sec. 5.

2. Theoretical model

The considered system is illustrated in Fig. 1. ADMR is subjected to Aharonov-Bohm flux, a lower ring consists of one type of atomic sites different from atomic sites in the upper ring.

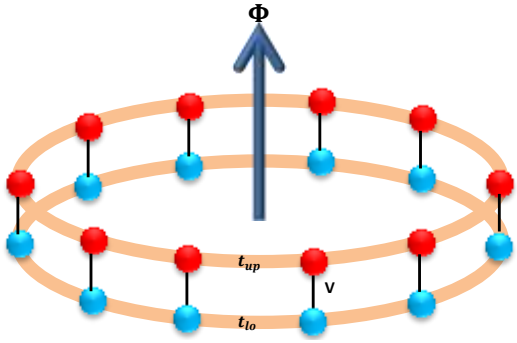

Fig. 1. Alloyed double metal ring, threaded by Aharonov-Bohm flux Φ, a lower ring consists of one type of atomic sites different from atomic sites in upper ring.

The tight binding Hamiltonian of the system is given by,

$$H = E_{up}\sum_i a_i^\dagger a_i + E_{lo}\sum_j b_j^\dagger b_j - t_{up}\sum_i (a_i^\dagger a_{i+1}e^{i\phi_{up}} + h.c) - t_{lo}\sum_i (b_i^\dagger b_{i+1}e^{i\phi_{lo}} + h.c) - V\sum_i (a_i^\dagger b_i + b_i^\dagger a_i) \quad (1)$$

where E_{up} and E_{lo} are the on-site energies of upper and lower rings, respectively, t_{up} and t_{lo} are the nearest-neighbor hopping strengths of

upper and lower rings, respectively. While V represents inter-ring coupling strength. $a_i^\dagger(a_i)$ and $b_j^\dagger(b_j)$ represent the creation(annihilation) operators for an electron at the atomic sites in upper and lower ring, respectively. The phase factors of ADMR are $\phi_\alpha = \frac{2\pi}{N_\alpha}\frac{\Phi}{\Phi_0}$, where $\alpha = up, lo$, Φ is magnetic flux threaded by upper and lower ring , $\Phi_0 = \mathrm{h}/e$ represents the elementary flux quantum, the number of atomic sites in each ring is N_α which will be equal in both rings ($N_\alpha = N_{up} = N_{lo}$).

1.3. Energy spectrum

In order to calculate the energy dispersion relation for ADMR, let us begin with Hamiltonian (1).

By using Fourier transforms can be rewritten Eq. (1) in k-space,

$$H = \sum_k a_k^\dagger\, a_k\left(E_{ou} - 2t_{up}\cos q_{up}a\right) + \sum_k b_k^\dagger\, b_k(E_{lo} - 2t_{lo}\cos q_{lo}a) - V\sum_k(a_k^\dagger\, b_k\, e^{ika} + b_k^\dagger a_k e^{-ika}), \qquad (2)$$

where $q_\alpha a = \frac{2\pi}{N_\alpha}\left(n + \frac{\Phi}{\Phi_0}\right)$ with $(\alpha = up, lo)$. The quantized values of wavevector k are given by $\frac{2\pi n}{Na}$, where a is the lattice spacing, n is a quantum number and it is restricted within the range: −N/2 ≤ n < N/2 [34].

The Eq. 2 can be written as a matrix,

$$H = \sum_k (a_k^\dagger\, , b_k^\dagger)\begin{pmatrix} E_{up} - 2t_{up}\cos q_{up}a & -Ve^{ika} \\ -Ve^{-ika} & E_{lo} - 2t_{lo}\cos q_{lo}a \end{pmatrix}\begin{pmatrix} a_k \\ b_k \end{pmatrix} \qquad (3)$$

The dispersion relations of ADMR can be given by,

$$E = \frac{(A+B) \pm \sqrt{(A-B)^2 + 4V^2}}{2}, \qquad (4)$$

where $A = E_{up} - 2t_{up}\cos q_{up}a$ and $B = E_{lo} - 2t_{lo}\cos q_{lo}a$

2.3. Persistent current

At absolute zero temperature (T =0 K), the persistent current in the ADMR described with fixed number of electrons N_e is determined by

$$I_n = -\frac{\partial E_0}{\partial \Phi} \quad (5)$$

where $E_0(\Phi)$ is the ground-state energy as a function of A-B flux Φ [21].

Once we get the energy eigenvalues as a function of flux Φ, we can easily calculate persistent current for individual energy eigenstates. It is simply the first order derivative of energy with respect to the flux. Therefore, for an n-th eigenstate we can write the expression for the current as,

$$I_n = \frac{1}{2}\left[\left(X_{up} + X_{lo}\right) \pm \frac{\left(X_{up} - X_{lo}\right)(A-B)}{\sqrt{(A-B)^2 + 4V^2}}\right] \quad (6)$$

where

$$X_\alpha = t_\alpha \frac{4\pi}{N_\alpha \Phi_0} sin\frac{2\pi}{N_\alpha}\left(n + \frac{\Phi}{\Phi_0}\right) \quad (7)$$

where, +ve or −ve sign in the current expression appears depending on the choice of n i.e., in which sub-band the energy level exists, with $n = 0, \mp 1, \mp 2, \ldots$ .At absolute zero temperature, total persistent current I for a particular filling N_e is obtained by taking the sum of individual contributions from the lowest N_e energy eigenstates [34]. Therefore, the total persistent current can be written as,

$$I_T = \sum_{n=1}^{N_e} I_n \quad (8)$$

There are many properties can be investigated in this study. These are including drude weight and Low-field magnetic susceptibility. The Drude weight is the second derivative of ground-state energy, which is given by,

$$D = \frac{N}{4\pi^2}\frac{\partial^2 E}{\partial \Phi^2} \quad (9)$$

While, low-field magnetic susceptibility at magnetic flux is given by,

$$\chi(\Phi) = \frac{N^3}{16\pi^2}\frac{\partial I(\Phi)}{\partial(\Phi)} \quad (10)$$

Evaluating the sign of $\chi(\Phi)$lead to predict whether the current is paramagnetic or diamagnetic in nature. Here we will determine $\chi(\Phi)$ only in the limit $\chi(\Phi) \rightarrow 0$ since we are interested to know the magnetic response in the low-field limit [35].

3. Computational method

In view of the good performance of density functional theory (DFT), we were instigated to perform DFT calculations at the B3LYP level of theory on all of the metal rings we studied using the standard Gaussian 09W software package and GaussView 5.0 program [36]. The geometries of all species were optimized at the Becke 3-parameter hybrid functional [37] combined with the Lee-Yang-Parr correlation functional, abbreviated as B3LYP level of density functional theory, using the LANL2DZ basis set.

4. Results and discussion

All energies and coupling strengths between subsystems were measured in units of $t_{lo} = 1eV$ where $c = e = h = 1$. All calculations achieved for non-interacting systems of electrons.

4.1. Energy spectrum

The energy spectrum of ADMR plotted as a function of the magnetic flux in Figs. 2-4 for different factors at zero temperature. The number of atomic sites in each ring is selected $N_{up} = N_{lo} = 10$, this means that the total size of ADMR is $N = N_{up} + N_{lo} = 20$. The parabola behavior of the energy levels as functions of the magnetic flux is still retained. The energy bands are symmetric in magnetic flux, due to the eigenenergies of ADMR are symmetric in the wavevectore. Energy levels in energy spectrum have maximum or minimum values with depends on the value of magnetic flux either half-integer or integer.

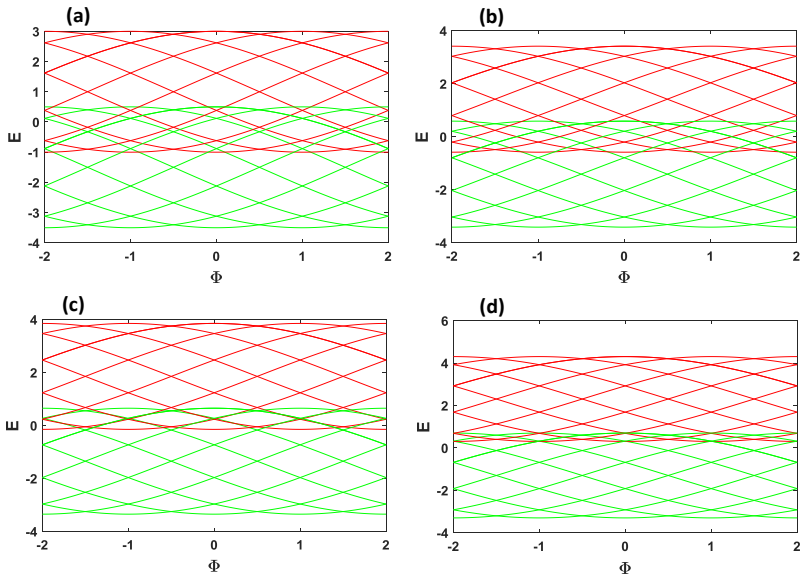

Fig. 2. Energy spectrum of double mesoscopic ring with $t_{up} = 1$, $E_{up} = -1$, V=1, and the number of sites in each ring N=10 (a) $E_{lo} = 0.5$, (b) $E_{lo} = 1$, (c) $E_{lo} = 1.5$, (d) $E_{lo} = 2$.

In Fig. 2, the energy spectrum as a function of magnetic flux presented for several values of $E_{lo} = 0.5,1,1.5,2$. The upper and lower energy bands shifted to the top and down, respectively. The upper energy band shifted by 0.4, while the lower energy band moves into down by 0.07. This means that changing the on-site energy E_{lo} greatly affects the upper energy band while its effect is slight on the lower energy band. This behavior reverses when E_{lo} is constant and E_{up} is changed.

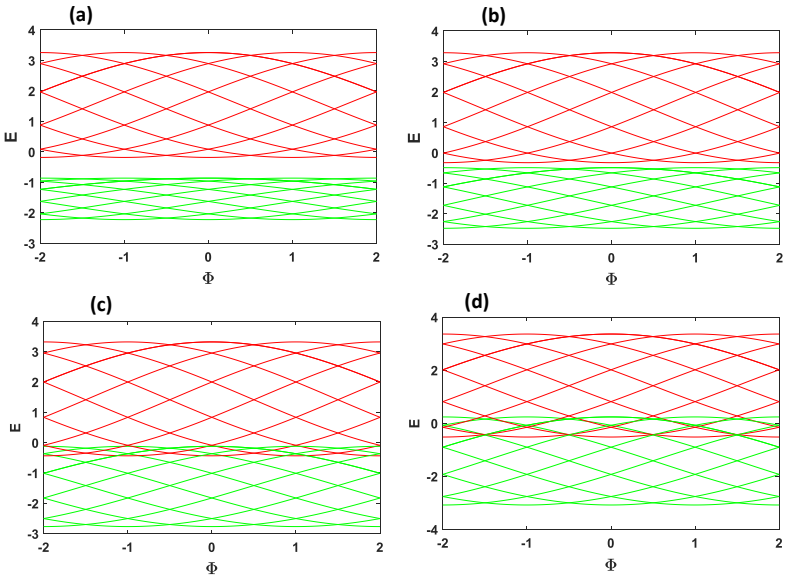

Fig. 3. Energy spectrum of double mesoscopic ring with $t_{up} = t_{lo} = 1$, $E_{up} = -1$, V=1, and the number of sites $N_{up} = N_{lo} = 10$, (a) $t_{up} = 0.2$, (b) $t_{up} = 0.4$, (c) $t_{up} = 0.6$, (d) $t_{up} = 0.8$.

While in Fig. 3, the range of the overlap zone obviously reduced as t_{up} decreased because bandwidth becomes narrow when t_{up} decreased. Noteworthy, energy spectrum shows that two different bands of energy levels were appeared, and they are separated by a finite energy gap. This energy gap is controllable by the two parameters. The first, energy gap decreases when nearest-neighbor hopping strength t_{up} increases due to the increasing the probability of hopping the electron from an atomic site to nearest neighbor with the same ring. The second, the increment of inter-ring coupling lead to decreasing of energy gap because the probability of hopping the electron from one ring to another ring will be increase, as illustrated in Fig. 4. To deeply understand the effect of inter-ring coupling strength on the behavior of the energy spectrum, it is presented in Fig. 4 for several values $= 0.5, 1, 1.5$ and 2 . The two energy bands symmetrically shifted into the top and down, but the magnitude of shift increases as follows 0.3, 0.4 and 0.45, when inter-ring coupling strength increases as follows $1, 1.5$ and 2.

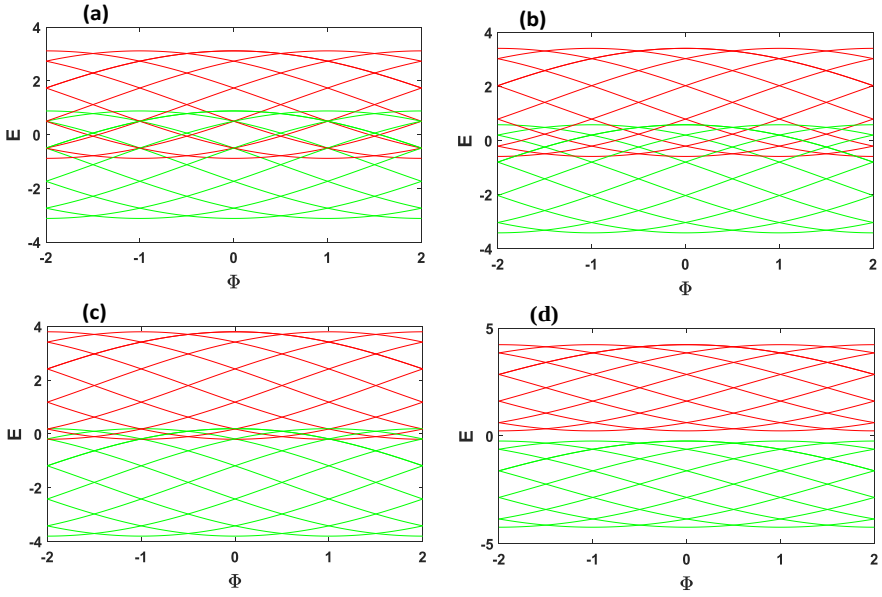

Fig. 4. Energy spectrum of double mesoscopic ring with $t_{lo} = t_{up} = 1$, $E_{lo} = -E_{up} = 1$, and the number of sites $N_{up} = N_{lo} = 10$, (a) V=0.5, (b) V=1, (c) V=1.5, (d) V=2.

4.2. Persistent current

The persistent current measured in units t_{lo}. The current-flux characteristics for ADMR are presented in Figs. 5-9. The size of each ring is $N_{up} = N_{lo} = 10$ with the number of electrons $N_e = 6,7,8\ and\ 9$ in all Figs. 5-7. The persistent current behaves as saw-tooth with sharp jumps at integer or half-integer multiples of flux-quantum Φ_0, respectively. This behavior can be obviously understood through the energy spectrum, we have seen that at integer or half-integer multiples of flux-quantum, energy levels have either a maximum or a minimum value, therefore it gives vanishing behavior of persistent current at these specific values of Φ. Because the current is obtained by taking the first order derivative of energy E(Φ) with respect to magnetic flux Φ. The amplitudes of current are clearly increasing when the on-site energies increase. The amplitude of persistent current become 3, 2.4, 1.7, 0.9 at E=0.8 for the number of electrons $N_e = 6,7,8\ and\ 9$, respectively as shown in Fig. 5.

The effect t_{up} on the amplitude of persistent current is presented in Fig. 6. The amplitude of current at $t_{up} = 0.8$ is up to 2.65, 2.25, 1.6 and 1.1 for the number of electrons $N_e = 6,7,8\ and\ 9$, respectively.

In Fig.7, the persistent current plotted for several values of inter-ring coupling strengths. The amplitude of persistent current at $V = 0.8$ is 2.5, 2.1, 1.5 and 0.8 for the number of electrons $N_e = 6,7,8\ and\ 9$, respectively.

The following observation shows the study of persistent current in non-half-filled and half-filled case for several values of $N_e = 6,16,26$ and $N_e = 7,17,27$ with ring size $N_{lo} = N_{up} = 26$ and $N_{lo} = N_{up} = 27$ as indicated in Figs. 8(a) and 8(b), respectively. Both results indicate that the amplitude of persistent current is increases when the number of electrons increases.

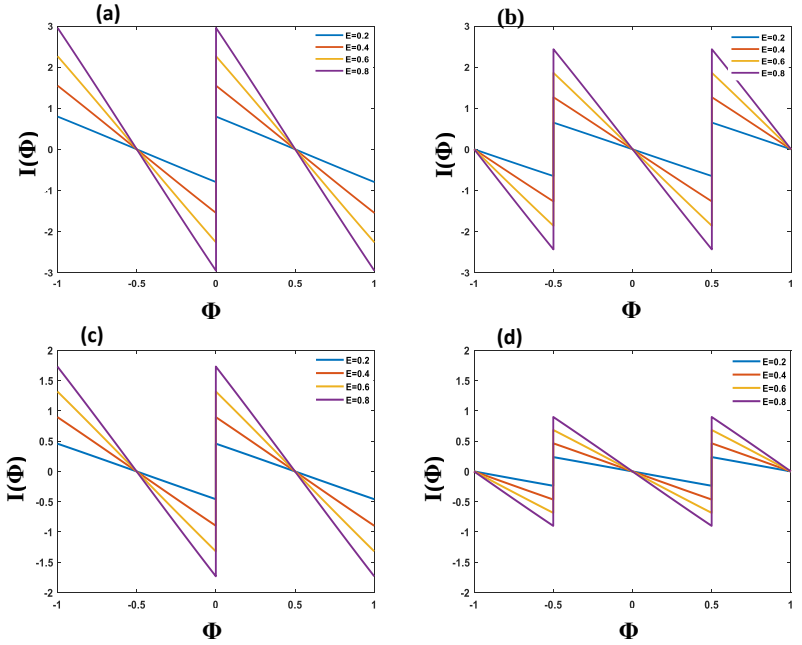

Fig. 5. Persistent current as a function of magnetic flux with $N_{up} = N_{lo} = 10$, $t_{lo} = 1, t_{up} = 0.5$, V=1, for several values of on-site energies $E_{lo} = -E_{up} = 0.2, 0.4, 0.6, 0.8$. The number of electrons are (a) $N_e = 6$ and (b) $N_e = 7$ (c) $N_e = 8$ (d) $N_e = 9$.

The electrons hop to the nearest neighbor sites depending on three important factors are t_{up}, V and E. Altogether these factors enhance electron hopping, which leads to conducting phase in non-half-filled case. While electron hopping reduced as these factors decrease. The half-filled case can be clearly observed at $N_e = 26$ and $N_e = 27$. The persistent current is completely vanishes at $N_e = 26$ and $N_e = 27$ for even and odd number of electrons, in half-filled case ($N_{lo} = N_{up} = 26$ and $N_{lo} = N_{up} = 27$), respectively. This case exhibits an insulating phase. The vanishing behavior of current can be understood as follows. The probability of hopping the electron to the neighboring sites will disappear because most atomic sites are occupied with electrons in half-filled case.

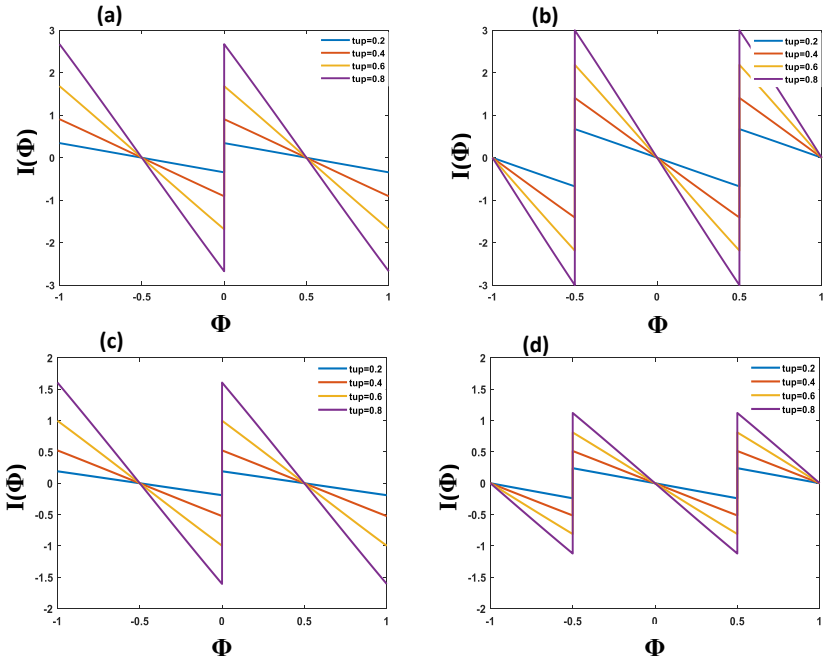

Fig. 6. Persistent current as a function of magnetic flux with $N_{up} = N_{lo} = 10$, $E_{lo} = -E_{up} = 1, t_{lo} = 1$, V=1 for several values of $t_{up} = 0.2, 0.4, 0.6, 0.8$. The number of electrons are (a) $N_e = 6$ and (b)$N_e = 7$ (c) $N_e = 8$ (d) $N_e = 9$.

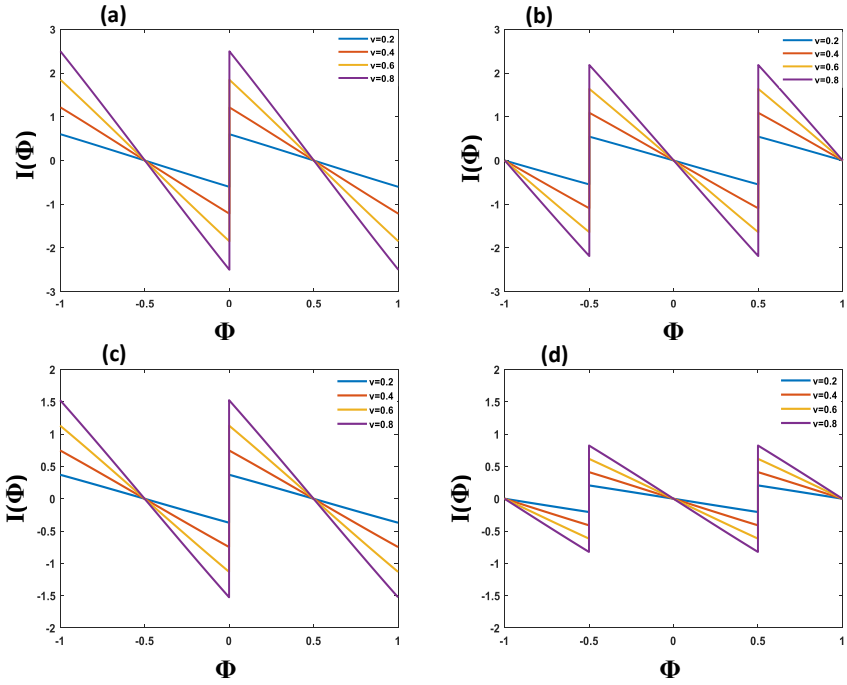

Fig. 7. Persistent current as a function of magnetic flux with $N_{up} = N_{lo} = 10$, $E_{lo} = -E_{up} = 1$, $t_{lo} = 1, t_{up} = 0.5$, for several values of V=0.2, 0.4, 0.6, 0.8 .The number of electrons are (a) $N_e = 6$ and (b)$N_e = 7$ (c) $N_e = 8$ (d) $N_e = 9$.

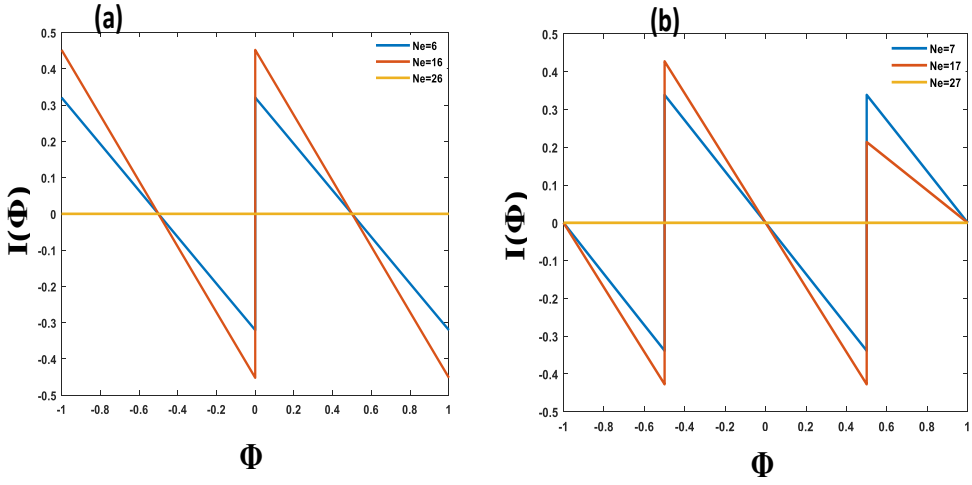

Fig. 8. Persistent current as a function of magnetic flux with $E_{lo} = -E_{up} = 1$, $t_{lo} = t_{up} = 1, V = 1$.The number of electrons are (a) even

$N_e = 6,16,26$ with $N_{lo} = N_{up} = 26$ and (b) odd $N_e = 7,17,27$ with $N_{lo} = N_{up} = 27$.

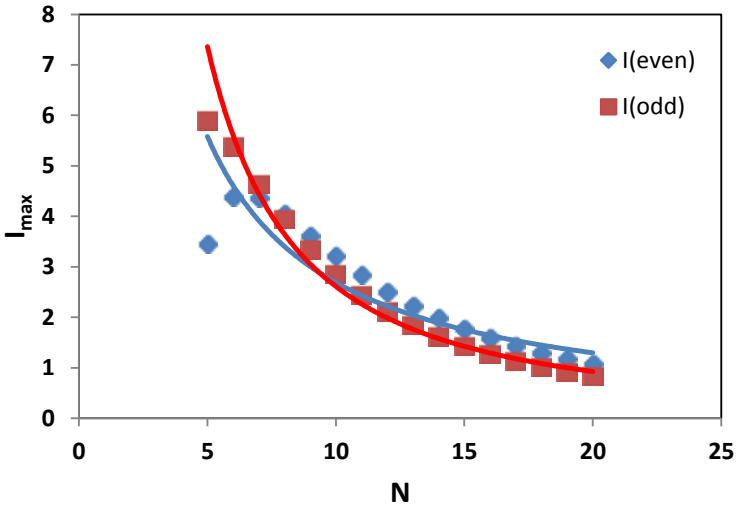

Fig. 9. Variation of persistent current as a function of ring size N with $E_{lo} = -E_{up} = 1, V = 1, t_{lo} = t_{up} = 1$. The even and odd number of electrons are analyzed depending on $N_e = 4$ and 3, respectively.

The variation of I_{max} as a function of ring size is presented in Fig. 9. The maximum absolute value of current amplitude I_{max} obtained from the current-flux curve as a function of ring size is presented in Fig. 10. A scaling relation $I_{max} = DN^{-\alpha}$ based by depending on the maximum absolute values of the current amplitude, in order to investigate asymptotic behavior of persistent current with ring size. The exponent α becomes 1.495 and 1.053 in case odd and even number of electrons, respectively. Whereas factor D depends on system size where D=81.629 and D=30.357 for the odd and even number of electrons, respectively. These curves show that persistent current decays algebraically with increasing system size.

4.3. Drude weight

In order to determine the nature of conducting of considered system, we presented the Drude weight as a function of the ring size in Fig. 10. The Drude weight curves for several values of $t_{up} = 0.2,0.4,0.6$ and 0.8 are calculated at N=4n+2 with the number of electrons $N_e = 10$ at $\Phi \to 0$. The curves are distinct at the small sizes of rings. However, the curves at t_{up} small are vanishing faster than that at t_{up} large. The vanishing

behavior of Drude weight shows the crossing of the system from the conducting phase to the insulating phase.

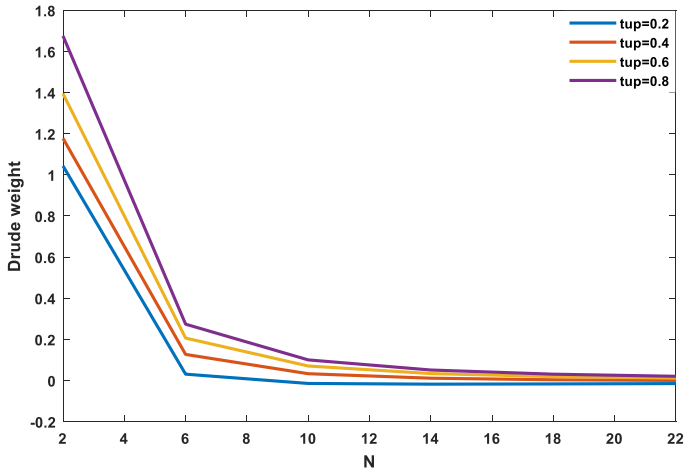

Fig. 10. Drude weight as a function of the ring size, $E_{lo} = -E_{up} = 1$, V=1, $t_{lo} = 1$, $N_e = 10$. For $t_{up} = 0.2, 0.4, 0.6, 0.8$.

4.4. Low-field magnetic susceptibility

The current can be controlled whether is paramagnetic or diamagnetic by calculating low-field magnetic susceptibility at $\Phi \to 0$. In Fig. 11, the total magnetic susceptibility with the quantum number n, which lies in the range $\frac{-N_e}{2} < n < \frac{N_e}{2}$, plotted as a function of N_e , where N_e represents the number of electrons. The low-field magnetic susceptibility has diamagnetic behavior at $\Phi \to 0$, which means only diamagnetic persistent current in ADMR. To understand this behavior, the Fig. 11 can be compared with Figs. 5(a) and 5(b), the persistent current has a negative slope at $\Phi = 0$, which means diamagnetic persistent current.

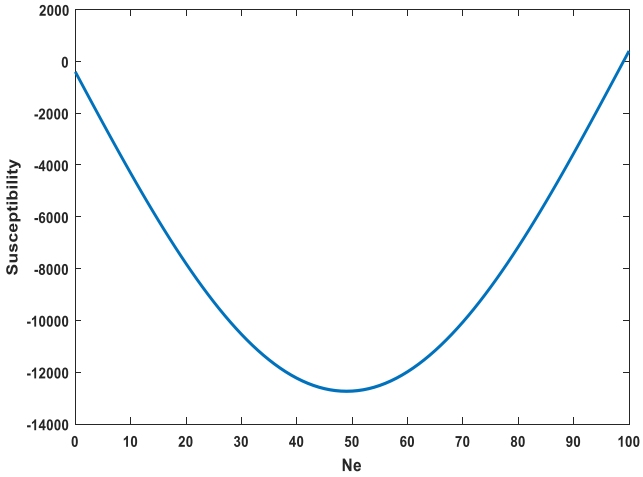

Fig. 11. Low-field magnetic susceptibility as a function of the number of electrons N_e , $E_{lo} = -E_{up} = 1$, V=1, $t_{lo} = t_{up} = 1$.

3.5. Results of DFT

Before proceeding with calculating electronic properties, it is necessary to get out the geometry optimization of the alloyed double metal rings. The equilibrium geometries for all studied systems were optimized at the DFT level of theory using a B3LYP functional together with the standard LANL2DZ basis set. In order to deeply understand the changes in electronic properties of the alloyed double metal rings, it is essential to plot the electronic density of state (DOS) of the alloyed double metal rings. The equilibrium geometries, DOS, HOMO plot and LUMO plot of the alloyed double metal rings Cu_6Au_6, Cu_6Ag_6, and Ag_6Au_6 are computed as shown in Fig. 12. Since the DOS is associated with the eigenenergies of the studied systems. The DOS is changed due to varying the metal type.

Type	HOMO	LUMO	DOS spectrum
(a) Cu_6Au_6			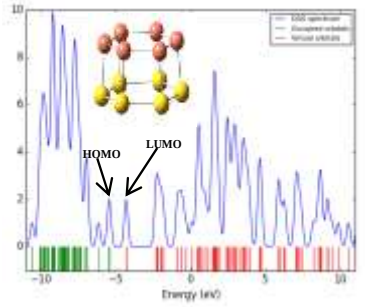
(b) Cu_6Ag_6			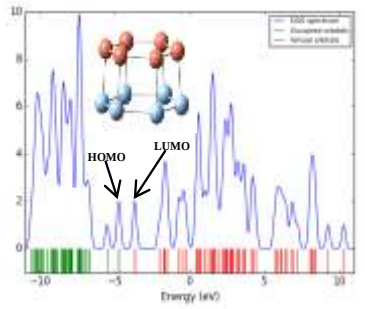
(c) Ag_6Au_6	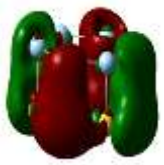	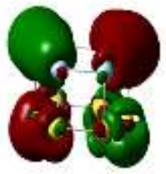	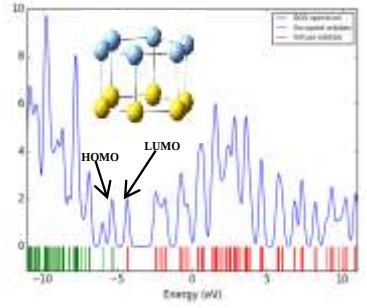

Fig. 12. Optimized structures, DOS spectrum, HOMO and LUMO plots of alloyed double metal rings (a) $Cu_6 Au_6$, (b) $Cu_6 Ag_6$ and (c) Ag_6Au_6.

The energy of HOMO is often associated with the electron donating ability of the studied system, whereas the energy of LUMO is associated with the electron accepting ability of the studied system. Therefore, the high value of HOMO shows a high contribution to donate electrons to adequate acceptor molecule with low empty molecular orbital energy. Likewise, the low value of LUMO shows a high contribution to accept electrons from the metal surface. The gap between the HOMO and

LUMO energy levels of the metal rings is another important character that should be studied. Large values of the energy gap mean high electronic stability and then low reactivity, but low values represent easily removing an electron from the HOMO orbital to LUMO, which can lead to good.

The energy gap between HOMO and LUMO determines the chemical stability of molecules. It is noted that the values of energy gap of alloyed double metal rings are close. The energy gap varies in the following order $Cu_6Au_6 > Cu_6Ag_6 > Ag_6Au_6$. Therefore, these molecules could be considered as the prototypical molecules for a whole series of cyclic all-metal-containing metallacycles, thus establishing an important new field in nanoelectronics.

Depending on HOMO and LUMO values for the studied systems, the global chemical reactivity descriptors, such as electronegativity, chemical hardness, chemical softness and electrophilicity are calculated as listed in Table 1. The chemical hardness and softness are very important parameters to describe the reactivity and stability of the molecules. Soft molecules are more reactive than hard ones because they can easily offer electrons. The Ag_6Au_6 ring acquired the highest value of chemical softness with respect to its counterparts because it has the lowest value of energy gap. Therefore, the Ag_6Au_6 ring may consider the more effective system. The high stability of the metal rings is also reflected on the high chemical hardness. According to the computed values, the stability of the metal rings increases in order $Cu_6Au_6 > Cu_6Ag_6 > Ag_6Au_6$. Notice that Ag_6Au_6 rings, having much higher values of the electrophilicity, than other rings, are stronger nucleophiles.

Table 1. The calculated data: HOMO energy, LUMO energy, energy gap E_g, electronegativity (χ), chemical hardness (η), electrophilicity (ω) and softness (S) for the alloyed double metal ring. All energies measured in eV units.

System	E_H	E_L	E_g	χ	η	ω	S
Cu_6Au_6	-5.421	-4.315	1.106	4.868	0.553	21.426	0.904
Cu_6Ag_6	-4.724	-3.669	1.055	4.196	0.527	16.704	0.948
Ag_6Au_6	-5.308	-4.328	0.979	4.818	0.489	23.735	1.022

The energy gap is a key factor to enhance the electrical conductivity of a material, as shown in following relation $\sigma\alpha\ exp\left(-\frac{E_g}{2k_BT}\right)$ [38, 39], where, $\sigma, k_B,$ and T, are the conductivity, the Boltzmann's constant, and the temperature 298.14 K, respectively. Reducing the energy gap is an important in the application of metal rings because of the new systems have more reactive in charge transfer process and have good semiconductor properties to use as nanoelectronic devices.

5. Conclusion

To summarize, the electronic properties of ADMR were examined in dependence on the magnetic flux, which threaded the system. The two different bands of energy levels are appearing in the energy spectrum, and they are separated by a finite energy gap. This energy gap is tunable by the two parameters are nearest-neighbor hopping t_{up} and inter-ring coupling (V) strengths.

The amplitudes of persistent current clearly influenced by the three parameters are on-site energy, nearest-neighbor hopping strength and inter-ring coupling strength. The on-site energy is considered a more effective parameter on the amplitude, while the inter-ring coupling strength is the less effective parameter on the amplitude.

The energy gap, chemical hardness and softness are very important parameters to describe the reactivity and stability of the studied systems. Furthermore, the energy gap shows the semiconductor characteristic of the studied systems. Thus, the Ag_6Au_6 ring may consider the more effective system. Therefore, these systems establish an important new field in nanoelectronics.

References

[1] J. Yi, J. Wei, J. Hong, S.-I. Lee, Giant persistent currents in the open Aharonov-Bohm rings, Physical Review B, 65 (2001) 033305.

[2] S. Washburn, R.A. Webb, Aharonov-Bohm effect in normal metal quantum coherence and transport, Advances in Physics, 35 (1986) 375-422.

[3] H.-F. Cheung, Y. Gefen, E.K. Riedel, W.-H. Shih, Persistent currents in small one-dimensional metal rings, Physical Review B, 37 (1988) 6050.
[4] S. Saha, S.K. Maiti, S. Karmakar, Conformation dependent magnetotransport in a single handed helical geometry, Physics Letters A, 379 (2015) 2848-2852.
[5] M. Büttiker, Y. Imry, R. Landauer, Josephson behavior in small normal one-dimensional rings, Physics letters a, 96 (1983) 365-367.
[6] M. Büttiker, Small normal-metal loop coupled to an electron reservoir, Physical Review B, 32 (1985) 1846.
[7] V. Meden, U. Schollwöck, Persistent currents in mesoscopic rings: A numerical and renormalization group study, Physical Review B, 67 (2003) 035106.
[8] A. Bleszynski-Jayich, W. Shanks, B. Peaudecerf, E. Ginossar, F. Von Oppen, L. Glazman, J. Harris, Persistent currents in normal metal rings, Science, 326 (2009) 272-275.
[9] H. Bluhm, N.C. Koshnick, J.A. Bert, M.E. Huber, K.A. Moler, Persistent currents in normal metal rings, Physical review letters, 102 (2009) 136802.
[10] V. Ambegaokar, U. Eckern, Coherence and persistent currents in mesoscopic rings, Physical review letters, 65 (1990) 381.
[11] W. Rabaud, L. Saminadayar, D. Mailly, K. Hasselbach, A. Benoit, B. Etienne, Persistent currents in mesoscopic connected rings, Physical Review Letters, 86 (2001) 3124.
[12] H.-F. Cheung, E.K. Riedel, Y. Gefen, Persistent currents in mesoscopic rings and cylinders, Physical review letters, 62 (1989) 587.
[13] O. Entin-Wohlman, Y. Gefen, Persistent currents in two-dimensional metallic cylinders: a linear response analysis, EPL (Europhysics Letters), 8 (1989) 477.
[14] S.K. Maiti, Magnetic responses in 1D mesoscopic rings and cylinders, Physica E: Low-dimensional Systems and Nanostructures, 31 (2006) 117-124.
[15] M. Saha, S.K. Maiti, Magnetic response of non-interacting and interacting electrons in a Möbius strip, Superlattices and Microstructures, 100 (2016) 1081-1093.

[16] X. Zotos, Finite temperature Drude weight of the one-dimensional spin-1/2 Heisenberg model, Physical review letters, 82 (1999) 1764.
[17] M. Omidi, E. Faizabadi, Temperature-related behavior of the persistent current in a zigzag hexagonal graphene ring, EPL (Europhysics Letters), 110 (2015) 17005.
[18] M. Omidi, E. Faizabadi, Electron–phonon interaction effect on persistent current in a one-dimensional quantum ring by using a simple model, Physics Letters A, 379 (2015) 1898-1901.
[19] S.K. Maiti, J. Chowdhury, S. Karmakar, On the role of electron correlation and disorder on persistent currents in isolated one-dimensional rings, Solid state communications, 135 (2005) 278-283.
[20] M. Patra, S.K. Maiti, Anomalous magnetic response of a quasi-periodic mesoscopic ring in presence of Rashba and Dresselhaus spin-orbit interactions, The European Physical Journal B, 89 (2016) 88.
[21] S.K. Maiti, M. Dey, S. Sil, A. Chakrabarti, S. Karmakar, Magneto-transport in a mesoscopic ring with Rashba and Dresselhaus spin-orbit interactions, EPL (Europhysics Letters), 95 (2011) 57008.
[22] S.K. Maiti, Persistent current in one-dimensional non-superconducting mesoscopic rings: effects of single hopping impurity, in-plane electric field and foreign atoms, International Journal of Modern Physics B, 22 (2008) 4951-4965.
[23] C.A. Tsipis, E.E. Karagiannis, P.F. Kladou, A.C. Tsipis, Aromatic Gold and Silver ‘Rings': Hydrosilver (I) and Hydrogold (I) Analogues of Aromatic Hydrocarbons, Journal of the American Chemical Society, 126 (2004) 12916-12929.
[24] S.D. Li, C.Q. Miao, G.M. Ren, D5h Cu5H5X: pentagonal hydrocopper cu5h5 containing pentacoordinate planar nonmetal centers (X= B, C, N, O), European Journal of Inorganic Chemistry, 2004 (2004) 2232-2234.
[25] X. Huang, S. Li, S. Wu, Y. Huang, F. Boey, C.L. Gan, H. Zhang, Graphene Oxide-Templated Synthesis of Ultrathin or Tadpole-Shaped Au Nanowires with Alternating hcp and fcc Domains, Advanced Materials, 24 (2012) 979-983.
[26] S. Rodríguez-Barrero, J. Fernández-Larrinoa, I. Azkona, L. López de Lacalle, R. Polvorosa, Enhanced performance of nanostructured coatings

for drilling by droplet elimination, Materials and Manufacturing Processes, 31 (2016) 593-602.
[27] Y. Oshima, A. Onga, K. Takayanagi, Helical gold nanotube synthesized at 150 K, Physical review letters, 91 (2003) 205503.
[28] J. Wu, P. Li, Y.-T.F. Pan, S. Warren, X. Yin, H. Yang, Surface lattice-engineered bimetallic nanoparticles and their catalytic properties, Chemical Society Reviews, 41 (2012) 8066-8074.
[29] P. Kapoor, A. Kumar, M. Sharma, J. Kumar, A. Kumar, P. Ahluwalia, Alloyed monolayers of Cu, Ag, Au and Pt in hexagonal phase: A comprehensive first principles study, Materials Science and Engineering: B, 228 (2018) 84-90.
[30] P. Kapoor, J. Kumar, A. Kumar, A. Kumar, P. Ahluwalia, Electronic, Mechanical, and Dielectric Properties of Two-Dimensional Atomic Layers of Noble Metals, Journal of Electronic Materials, 46 (2017) 650-659.
[31] X. Ye, H. Shi, X. He, Y. Yu, D. He, J. Tang, Y. Lei, K. Wang, Cu–Au alloy nanostructures coated with aptamers: a simple, stable and highly effective platform for in vivo cancer theranostics, Nanoscale, 8 (2016) 2260-2267.
[32] S.S. Shankar, A. Rai, A. Ahmad, M. Sastry, Rapid synthesis of Au, Ag, and bimetallic Au core–Ag shell nanoparticles using Neem (Azadirachta indica) leaf broth, Journal of colloid and interface science, 275 (2004) 496-502.
[33] Y. Sakai, H.-J. Schneider-Muntau, Ultra-high strength, high conductivity Cu-Ag alloy wires, Acta Materialia, 45 (1997) 1017-1023.
[34] P. Dutta, S.K. Maiti, S. Karmakar, Magneto-transport in a binary alloy ring, Physics Letters A, 376 (2012) 1567-1572.
[35] S.K. Maiti, Magnetic response in mesoscopic Hubbard rings: A mean field study, Solid State Communications, 150 (2010) 2212-2217.
[36] A. Frisch, M. Frisch, F. Clemente, G. Trucks, Gaussian 09 User's Reference, Version 8.0, Gaussian: Wallingford, CT, (2009).
[37] A.D. Becke, Density-functional thermochemistry. III. The role of exact exchange, The Journal of chemical physics, 98 (1993) 5648-5652.
[38] S.S. Li, Semiconductor physical electronics, Springer Science & Business Media, 2012.

[39] A.D. McNaught, A. Wilkinson, Compendium of chemical terminology. Vol. 1669, in, Oxford: Blackwell Science, 1997.